

Synthesis of near infrared-reflective Mo-doped $\text{Sm}_2\text{Ce}_2\text{O}_7$ yellow pigment and near infrared-reflective glazes

Mantana Suwan^a, Paveena Premjit^a, Parjaree Thavorniti^a, Pinit Kidkhunthod^b and Sitthisuntorn Supothina^{a,*}

^aNational Metal and Materials Technology Center (MTEC), National Science and Technology Development Agency (NSTDA), 114 Thailand Science Park, Phahonyothin Rd., Klong Luang, Pathum Thani 12120, Thailand

^bSynchrotron Light Research Institute (Public Organization), 111 University Avenue, Muang District, Nakhon Ratchasima 30000, Thailand

Near infrared (NIR)-reflective Mo-doped $\text{Sm}_2\text{Ce}_2\text{O}_7$ yellow pigment was synthesized by solid-state reaction of the Sm_2O_3 and CeO_2 in the presence of the $(\text{NH}_4)_6\text{Mo}_7\text{O}_{24}$. All the raw materials were wet-milled in acetone for 6 hrs to achieve the homogeneous slurry followed by drying and firing at 1100, 1300 and 1500 °C for 6 hrs. The effect of Mo doping was investigated by adding 10, 15, 20, 25 and 30 wt.% $(\text{NH}_4)_6\text{Mo}_7\text{O}_{24}$ with respect to the CeO_2 . Extended X-ray absorption fine structure (EXAFS) analysis revealed the substitution of the Mo^{6+} for the Ce^{4+} . The doping resulted in a change of product's color; it turned from ivory white to yellow with the increase of dopant content up to 20 wt.%, and became dark green at higher doping level. With the increase of firing temperature from 1100 °C to 1500 °C, the color became brighter yellow due to more substitution of the Mo^{6+} for the Ce^{4+} . At the optimum synthesis condition, *i.e.* 20 wt.% doping level and 1500 °C firing, the product was most yellowish and had 69.2% NIR reflectance. This NIR-reflective pigment was mixed with a traditional glaze and waste-derived glaze. The resultant NIR-reflective glazes had very good chemical resistance with good appearance. The NIR reflectance increased from 50.7 to 59.7% for the traditional ceramic glaze, and from 31.5 to 42.3% for the waste-derived glaze.

Key words: Reflective pigment, Complex inorganic color pigment, Glaze, Solid-state reaction, Near-infrared reflectance.

Introduction

Urbanization has been a megatrend for the 21st century as most large cities have expanded rapidly. Around half of the world's human population lives in urban areas, and number of megacity, with over 10 million inhabitants, is increasing around the world. Such a rapid expansion of urban areas inevitable brings with it an increase in concrete infrastructure and an increase on demand for energy consumption especially for air-conditioning systems. Heat accumulated in surroundings caused by the heat released by cars, air-conditioning systems, buildings and pavements has a significant impact on the 'urban heat island (UHI) effect' which is characterized by higher air temperatures in the densely built areas than those of the surrounding rural areas. The increased urban temperature intensifies the use of a large amount of overall cooling load for air conditioning, the demand for peak electricity and the amount of greenhouse gases in the atmosphere [1-4]. This problem can be reduced by increasing the green areas, selecting a proper design of the buildings for

better air circulation and by using suitable building envelopes such as insulating walls and roofs. These actions can reduce the heat built-up inside the buildings.

Recently, solar-reflective roofs which can be fabricated by coating their surfaces with high-solar reflective pigments. Titanium dioxide (TiO_2) is an example of a typical white pigment with the near-infrared (NIR) solar reflection of about 90%. However, the use of the white pigment is a very rare case for roofing due to its less aesthetic appearance. Colored solar-reflective roofs have been recently introduced [5-13]. The roofs have been fabricated by coating their surfaces with non-white, high NIR-reflective pigments of the desired color. The solar-reflective pigments of various colors, such as green [7], yellow-brown [9-12], and reddish brown and reddish orange [13], have been synthesized.

Most of the pigments mentioned earlier are complex oxide compounds. The desired colors were obtained by doping suitable dopants into the parent oxide compounds. For instance, doping the Si^{4+} into the $\text{Y}_6\text{MoO}_{12}$ resulted in bright yellow color while doping with the Pr^{4+} resulted in red-brown color [12]. Similarly, yellow color was obtained by doping the $\text{Sm}_2\text{Ce}_2\text{O}_7$ with the Mo^{6+} while brown color was obtained by doping it with the Pr^{4+} [10]. For these materials, XRD patterns of the undoped and doped ones are very similar. Thus, the XRD analysis cannot effectively be utilized to investigate the

*Corresponding author:
Tel : +662-564-6500
Fax: +662-564-6447
E-mail: sitthis@mtec.or.th

doping reaction.

Therefore, one of the objectives of this study is to investigate the effect of Mo doping on local structure of the host $\text{Sm}_2\text{Ce}_2\text{O}_7$ by using the EXAFS analysis. In addition, the synthesized NIR-reflective yellow pigment was mixed with traditional ceramic glaze and the glaze derived from recycled fly ash and glass cullet. The resultant glazes were characterized for their physical property, and evaluated for their ability to reflect NIR radiation.

Experimental

Materials Preparation

The $\text{Sm}_2\text{Ce}_2\text{O}_7$ was synthesized by solid-state reaction of the samarium oxide (Sm_2O_3 , C.K. Ceramics Co., Ltd.) and cerium oxide (CeO_2 , C.K. Ceramics Co., Ltd.) at a molar ratio of the Sm_2O_3 : CeO_2 of 1 : 2 (or 50:50 by weight). The effect of the Mo^{6+} doping was investigated by adding 10, 15, 20, 25 and 30 wt.% ammonium molybdate ($(\text{NH}_4)_6\text{Mo}_7\text{O}_{24}$, C.K. Ceramics Co., Ltd.) based on the CeO_2 weight. All the raw materials were mixed together by wet milling in acetone to obtain a homogenous mixing, followed by drying at 100 °C and calcination at 1100, 1300 or 1500 °C for 6 hrs in an electrical furnace. The synthesized products were washed, ground and sieved through a 325-mesh sieve.

NIR-reflective glazes were prepared from 2 base glazes; one is a traditional ceramic glaze, the other is a waste-derived glaze. The wastes used were fly ash from a coal-fired power plant situated in Lampang province, the northern of Thailand, and the waste glass from the glass industry. Huge amounts of these wastes are generated each year and their disposal causes both economic and environmental impacts. The fly ash mainly consists of SiO_2 , Al_2O_3 , CaO and Fe_2O_3 which are common raw materials of ceramics. Thus, re-utilization of these wastes is a sustainable alternative to reduce both the consumption of natural resource and environmental impact. In this work, the wastes were used to replace natural raw materials and frit in a

proportion of 70 wt.%. Batch compositions of the glazes employed are shown in Table 1. The NIR-reflective glazes were prepared by mixing 20 wt.% NIR-reflective pigment with the glaze's raw material. The mixtures were milled in a planetary mill for 30 min and the obtained slips were passed through a 200-mesh sieve. The glaze slips were applied onto ceramic specimens, and then fired in an electrical furnace at 1150 °C with a soaking time of 15 min.

Characterizations

Crystal structure of the NIR-reflective pigments was identified by using XRD patterns acquired on the X'Pert PRO diffractometer (PANalytical). Diffused reflectance spectra of the NIR-reflective pigments and glazes were acquired on a Cary 5000 UV-Vis-NIR spectrophotometer (Agilent Technologies) in the wavelength range of 300 to 2100 nm. The reflectance was calculated following the ASTM standard (number G173-03). Band-gap energy (E_g) was calculated from the diffused reflectance spectra. The wavelength at the absorption edge was adopted for the approximation of the band-gap energy according to $E_g = hc/\lambda$, where h is the Planck's constant (6.626×10^{-34} J · s), and c is the speed of light (3.0×10^8 m/s). The CIE 1976 $L^*a^*b^*$ colorimetric method was employed for color measurement using the spectrophotometer (Konica Minolta, CM-2600d). In this method, the L^* axis represents the lightness (0 = black, 100 = white), the a^* axis represents the green (negative value) to red (positive value), and the b^* axis represents the blue (negative value) to yellow (positive value).

Mo doping in $\text{Sm}_2\text{Ce}_2\text{O}_7$ was revealed by the EXAFS analysis. The EXAFS measurements were acquired at "the SUT-NANOTEC-SLRI XAS Beamline (BL 5.2), Synchrotron Light Research Institute (Public Organization), Thailand". The Ce L3-edge EXAFS spectra of all samples were collected in the transmission mode. A Ge (220) double crystal monochromator with an energy resolution ($\Delta E/E$) of 2×10^{-4} was used to scan the synchrotron X-ray in a range of 5500-6100 eV. The photon energy was calibrated against the Ce L3-edge of the CeO_2 standard powder.

Properties of the NIR-reflective glazes were characterized as follow. Thermal expansion was measured at temperature ranging from 50 °C to 500 °C by using a dilatometer (Netzch, DIL 402 PC) at a heating rate of 10°C/min. The thermal expansion coefficient (α) was determined as:

$$\alpha = \frac{1}{L_0} \frac{\Delta L}{\Delta T} \quad (1)$$

where L_0 is the initial length of the test piece, ΔL is the change in length of the test piece and ΔT is the change in temperature.

Chemical resistance evaluation was performed with solutions of 3% hydrochloric acid (HCl), 10 g/l citric acid ($\text{C}_6\text{H}_8\text{O}_7$) and 30 g/l potassium hydroxide (KOH) following the ISO 10545-13 standard. The samples

Table 1. Composition of the traditional and waste-derived glazes.

| Raw materials | Amount (wt.%) | |
|--|-------------------|---------------------|
| | Traditional glaze | Waste-derived glaze |
| Na feldspar | 31 | – |
| CaCO_3 | 17 | – |
| BaCO_3 | 8 | – |
| ZnO | 5 | – |
| Kaolin | 10 | – |
| SiO_2 | 29 | – |
| MSWI fly ash | – | 30 |
| $\text{Na}_2\text{B}_4\text{O}_7 \cdot 10\text{H}_2\text{O}$ | – | 30 |
| Glass cullet | – | 40 |

were soaked at room temperature in $C_6H_8O_7$ solution for 24 hrs, followed by HCl solution for 96 hrs and KOH solution for 96 hrs, respectively. During the test with HCl and KOH, the solutions were replaced with new solutions after 48 hrs. Finally, after washing with water the samples were visually observed to evaluate the changes of their surface appearance.

Results and Discussion

XRD analysis of the samples synthesized at $1100\text{ }^\circ\text{C}$ for 6 hrs revealed weak reflection peaks which were well matched with the $Sm_2Ce_2O_7$. With the increase of calcination temperature to $1300\text{ }^\circ\text{C}$, intensities of these reflection peaks increased, while those of the starting raw materials decreased accordingly, indicating more solid-state reaction at higher calcination temperature. In contrast, an XRD pattern of the sample calcined at $1500\text{ }^\circ\text{C}$ (Fig. 1, undoped Mo) shows strong reflection peaks of the $Sm_2Ce_2O_7$, and no peaks of the Sm_2O_3 , CeO_2 and other impurities were observed, indicating completed

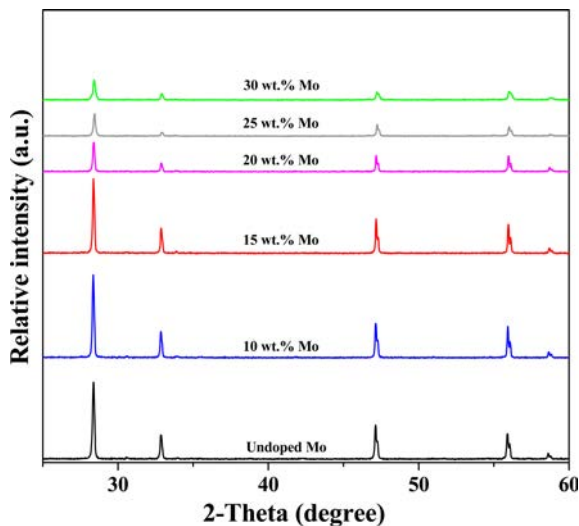


Fig. 1. XRD patterns of the undoped and Mo-doped samples calcined at $1500\text{ }^\circ\text{C}$ for 6 hrs.

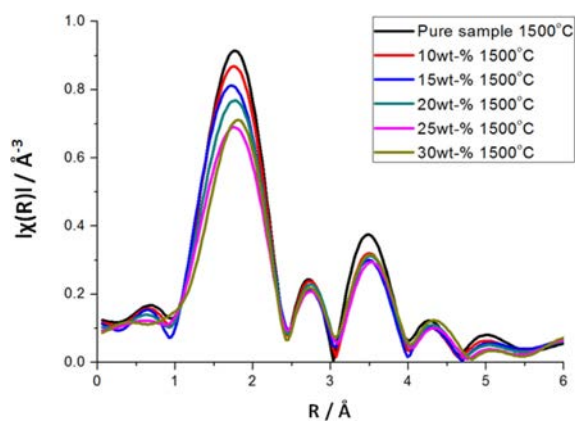


Fig. 2. The corrected and normalized EXAFS data in R-space of Ce L3-edge for all the Mo-doped $Sm_2Ce_2O_7$ samples (without phase shift) at various Mo contents.

solid-state reaction of pure $Sm_2Ce_2O_7$. According to Fig. 1, XRD patterns of the Mo-doped samples are very similar to that of the undoped sample, and thus the peaks of the parent and Mo-doped $Sm_2Ce_2O_7$ cannot be explicitly resolved by the XRD analysis. Nevertheless, the EDS analysis (not shown) revealed the presence of the Mo which increased upon the increase of the $(NH_4)_6Mo_7O_{24}$ that was mixed into the starting raw materials.

The EXAFS analysis was performed to further investigate the effect of Mo doping on the parent $Sm_2Ce_2O_7$, and the results are shown in Fig. 2. The effects on local structure around the Ce atoms due to the Mo doping (10, 15, 20, 25 and 30 wt.% $(NH_4)_6Mo_7O_{24}$ of the starting raw material) in the $Sm_2Ce_2O_7$ were also addressed by the EXAFS results. The EXAFS analysis including background correction of the measured EXAFS spectra was performed using the ATHENA program in the IFEFFIT package [14-15]. Figs. 2 and 3 show the corrected and normalized EXAFS data in the R-space of the Ce L3-edge for all the $Sm_2Ce_{2-x}Mo_xO_{7+\delta}$ samples (without the phase shift). According to Fig. 2, at calcination temperature of $1500\text{ }^\circ\text{C}$, the height of the first peak (Ce-O bonding coordination) tends to be slightly decreased when the Mo contents are increased. This is due to a decreased number of the first neighboring oxygen atoms around the Ce ions in the host structure suggesting that the cluster size of the Ce ions is decreased with the increase of the Mo content. Noted that the cluster size in this work is defined by two terms; a number of the first neighboring oxygen atoms around the Ce ions and the bonding length of the Ce-O. As the number of the first oxygen neighboring atoms and the bonding length around the Ce ions decrease, the cluster size of the Ce atom is reduced. Moreover, according to Fig. 3, at 20 wt.% doping, the height of the first peak tends to be slightly decreased when the calcination temperature was raised from $1100\text{ }^\circ\text{C}$ to $1500\text{ }^\circ\text{C}$, respectively. Also,

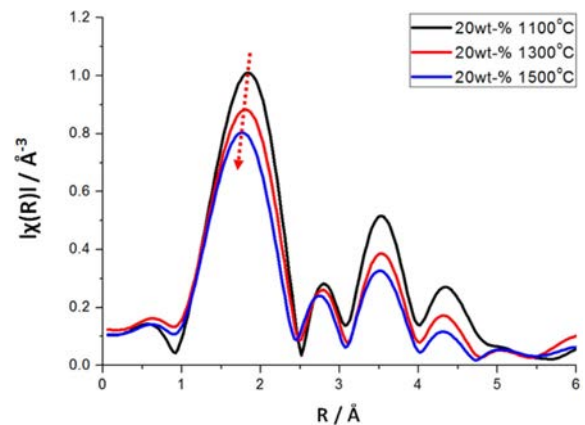


Fig. 3. The corrected and normalized EXAFS data in R-space of Ce L3-edge for all the Mo-doped $Sm_2Ce_2O_7$ samples (without phase shift) at 20 wt% $(NH_4)_6Mo_7O_{24}$ in samples.

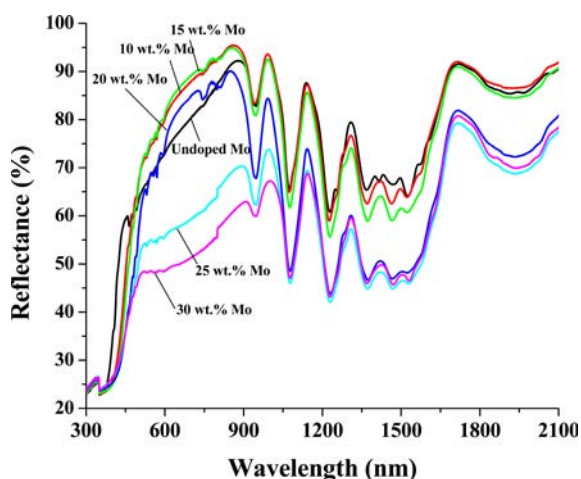


Fig. 4. Diffused reflectance spectra of the samples synthesized at 1500 °C at various doping levels.

the peak positions (Ce-O bonding distances) of the first peak are slightly decreased from 1.84 Å to 1.76 Å (without the phase shift) when the calcination temperature was raised from 1100 °C to 1500 °C, respectively. All of the effects observed by EXAFS analysis can be ascribed to the Mo substitution at the Ce sites in the host structure where the ionic radius of the Mo^{6+} (0.59 Å) is smaller compared to that of the Ce^{4+} (0.97 Å) [16].

In addition, the X-ray absorption near edge structure (XANES) spectra at the Mo and Ce L3-edge of the samples with various Mo contents were analysed. There was no significant difference among all the spectra suggesting that the oxidation states of the Mo atoms in all the samples are the same. Moreover, at the Ce L3-edge, the XANES features of all the samples were similar with a slight difference in the double peak height (at 5725 and 5735 eV) comparing with the pre-edge position. In more detail, the double peak height was reduced when the Mo contents were increased. Therefore, this XANES result can be used to support the EXAFS result for the substitution of the Ce atoms by the Mo atoms.

Fig. 4 shows the UV-Vis diffused reflectance spectra of the undoped and Mo-doped $\text{Sm}_2\text{Ce}_2\text{O}_7$. The reflectance spectrum of the undoped $\text{Sm}_2\text{Ce}_2\text{O}_7$ reveals a strong absorption at the wavelength below 450 nm which could be attributed to the O_{2p} - Ce_{4f} charge transfer transitions of the Ce ions [17-18]. The absorption in this region is responsible for the ivory white appearance of the undoped $\text{Sm}_2\text{Ce}_2\text{O}_7$. Upon the increase of Mo^{6+} doping, the absorption edge shifts toward higher wavelengths, from approximately 450 to 510 nm, due to the O_{2p} - Mo_{4d} charge transfer transitions [18]. The shift of the absorption edge is responsible for the change of the color from ivory white to yellow with the progressive doping of the Mo^{6+} .

The reflectance of the pigments after calcination at 1100, 1300 and 1500 °C at various Mo^{6+} doping levels

Table 2. Reflectance of the pigments after calcination at 1100, 1300 and 1500 °C at various doping levels.

| $(\text{NH}_4)_6\text{Mo}_7\text{O}_{24}$ content (wt.%) | Reflectance (%) | | |
|--|-----------------|---------|---------|
| | 1100 °C | 1300 °C | 1500 °C |
| 0 | 88.5 | 86.1 | 80.3 |
| 10 | 88.3 | 85.7 | 81.2 |
| 15 | 85.8 | 84.5 | 79.4 |
| 20 | 85.8 | 85.6 | 69.2 |
| 25 | 86.0 | 83.8 | 60.2 |
| 30 | 85.8 | 84.2 | 57.5 |

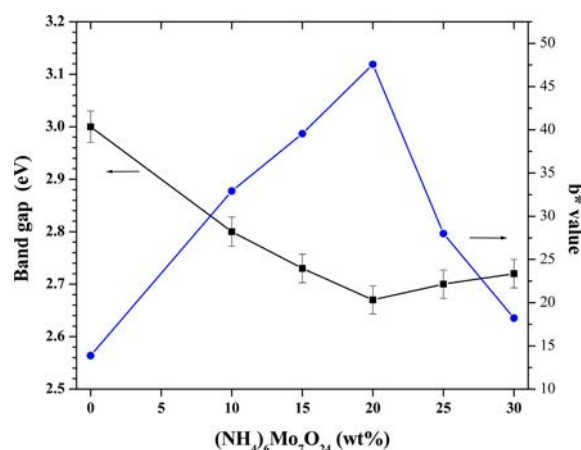


Fig. 5. Band-gap energy and b^* value of the samples synthesized at 1500 °C at various doping levels.

is shown in Table 2. No dramatic change of the NIR reflectance was observed after calcination at 1100 and 1300 °C at all Mo doping levels. This result is in good agreement with the result of crystal structure analysis that the Mo-doped $\text{Sm}_2\text{Ce}_2\text{O}_7$ did not completely form at 1100 and 1300 °C. Calcination at 1500 °C resulted in a reduction of the NIR reflectance to 57.5% at 30 wt.% Mo doping level due to the color change from ivory white to yellow to dark green upon the increase of the Mo doping. At the synthesis condition in which the pigment has the brightest yellow hue, *i.e.* 20 wt.% doping and 1500 °C, the NIR reflectance was 69.2%. A dramatic change of the color and the reflectance observed at the high synthesis temperature can be attributed to the substitution of the Mo^{6+} for the Ce^{4+} in the $\text{Sm}_2\text{Ce}_2\text{O}_7$ as revealed by the EXAFS analysis which alters its band-gap structure.

Fig. 5 shows the band gap and b^* value of the samples synthesized at 1500 °C at various doping levels. With the Mo doping, the band-gap energy gradually decrease from 3.0 eV for the undoped sample to about 2.7 eV for the samples with the Mo doping level of 20 wt.% or higher. Note that the band-gap energies at 20, 25 and 30 wt.% Mo doping are comparable within the experimental error. In the other word, increasing the Mo doping to more than 20 wt.%

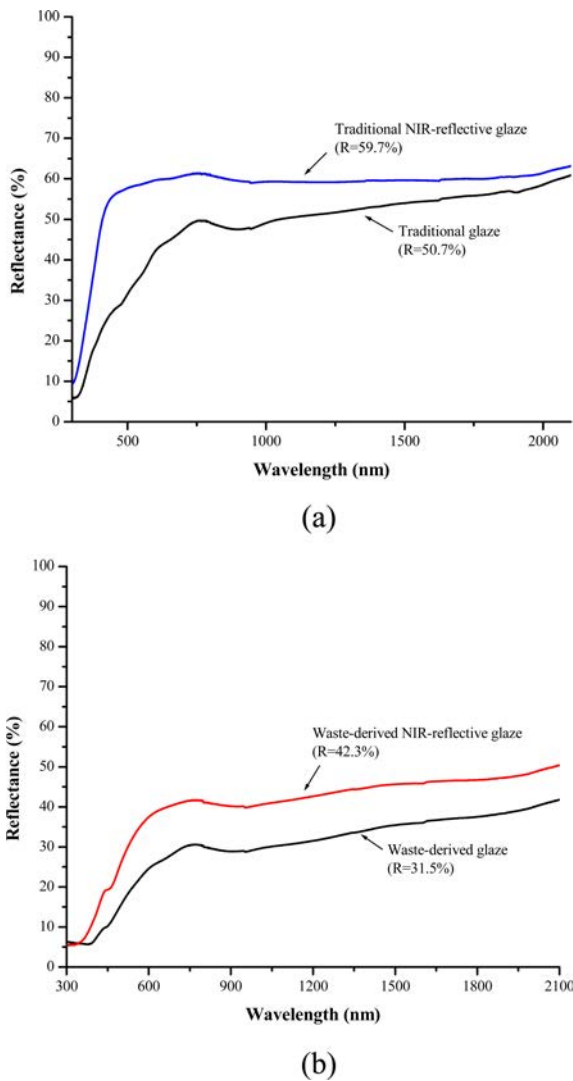


Fig. 6. Reflectance spectra of (a) the traditional NIR-reflective glaze and (b) the waste-derived NIR-reflective glaze.

did not have a dramatic effect on the band-gap energy. The b^* value which is an indicative of the yellow color significantly increases from the undoped sample (ivory white), reaching the maximum value at the doping level of 20 wt.% (bright yellow), and significantly decreases afterward (dark green). The change of the pigment's color can be ascribed to the decrease of the band-gap energy that alters the absorption of light.

Fig. 6(a) shows reflectance spectra of the traditional glaze and the traditional glaze consisting 20 wt.% NIR-reflective pigment. NIR reflectance of the traditional glaze calculated according to the ASTM G173-03 at the wavelength range of 780-2100 nm was 50.7%. The addition of NIR-reflective pigment into this glaze gave rise to the increase of NIR reflectance to 59.7%. Similarly, the waste-derived glaze had NIR reflectance of 28.7%, and its NIR reflectance can be raised to 42.3% by the addition of 20 wt.% NIR-reflective pigment as shown in Fig. 6(b). Both traditional and

Table 3. L^* , a^* , b^* parameter of the NIR-reflective glazes.

| | L | a^* | b^* |
|------------------------------------|-------|-------|-------|
| Waste-derived NIR-reflective glaze | 80.39 | 0.34 | 3.55 |
| Traditional NIR-reflective glaze | 59.31 | 3.12 | 19.52 |

Table 4. Thermal expansion coefficients of the NIR-reflective glazes and ceramic bodies.

| | Coefficient of Thermal Expansion ($^{\circ}\text{C}^{-1}$) at 50-500 $^{\circ}\text{C}$ |
|------------------------------------|---|
| Waste-derived NIR-reflective glaze | 11.84×10^{-6} |
| Traditional NIR-reflective glaze | 7.73×10^{-6} |
| Low-temperature ceramics | 11.69×10^{-6} |
| Tiles | $7.5-9.0 \times 10^{-6}$ |

Table 5. Chemical resistance of the NIR-reflective glazes.

| | HCl | $\text{C}_6\text{H}_8\text{O}_7$ | KOH |
|------------------------------------|------------------|----------------------------------|------------------|
| Waste-derived NIR-reflective glaze | no visual effect | no visual effect | no visual effect |
| Traditional NIR-reflective glaze | no visual effect | no visual effect | no visual effect |

waste-derived glazes (references) are transparent and glossy. The addition of NIR-reflective pigment resulted in less glossy appearance (higher matt appearance; the higher NIR-reflective pigment content, the higher matt appearance) due to less proportion of SiO_2 in the formulation. Their colorimetric parameter (L^* , a^* , b^*) are summarized in Table 3. The traditional NIR-reflective glaze has slightly more yellowish color hue as indicated by its more positive value of the b^* parameter.

Table 4 shows values of thermal expansion coefficients (α) of the NIR-reflective traditional glaze and NIR-reflective waste-derived glaze. Thermal expansion coefficients of ceramics and tiles are also given. The traditional NIR-reflective glaze has thermal expansion coefficient of $7.73 \times 10^{-6} \text{ }^{\circ}\text{C}^{-1}$ which is in the same range of thermal expansion coefficient of tiles. Thus, it can be used for conventional tile body. Lower thermal expansion coefficient of this glaze can be attributed to the existence of ZnO and the smaller amount of alkaline oxides in the composition. Higher thermal expansion coefficient of $11.84 \times 10^{-6} \text{ }^{\circ}\text{C}^{-1}$ was obtained from the waste-derived NIR-reflective glaze which well matches the coefficient of low-temperature ceramics. Note that it is important for the glaze and the body to be coated to have comparable thermal expansion coefficient to avoid crack and crazing of the glaze due to thermal expansion coefficient mismatch. Results of chemical resistance evaluated by sequential soaking in $\text{C}_6\text{H}_8\text{O}_7$, HCl and KOH solutions for 24, 96 and 96 hrs, respectively, are summarized in Table 5. No corrosive damage and other visual effects were observed on

surfaces of both NIR-reflective glazes, indicating very good resistance to acid and base.

Conclusions

The Mo-doped $\text{Sm}_2\text{Ce}_2\text{O}_7$ solar-reflective pigment was synthesized by solid-state reaction of the Sm_2O_3 and CeO_2 . The $(\text{NH}_4)_6\text{Mo}_7\text{O}_{24}$ was mixed with the raw material at 10-30 wt.% with respect to the CeO_2 to investigate the effect of Mo doping. The formation of the Mo-doped $\text{Sm}_2\text{Ce}_2\text{O}_7$ yellow pigment was promoted at high calcination temperature as well as high Mo doping level. The color of the synthesized pigments changed from ivory white to bright yellow with the NIR reflectance of 69.2% at the optimum synthesis condition of 1500 °C and 20 wt.% Mo doping. Higher doping level resulted in the reduced NIR reflectance. The evidence of Mo substitution at the Ce sites in the structure has been confirmed by the EXAFS analysis. Addition of the NIR-reflective pigment into the glazes dramatically enhanced their NIR reflectance. They had very good chemical resistance, and showed good appearance and matt surface. Based on their thermal expansion coefficients, the traditional NIR-reflective glaze can be used for tiles, and the waste-derived glaze can be used for low-temperature ceramics.

Acknowledgments

The authors would like to acknowledge the National Metal and Materials Technology Center, the National Science and Technology Development Agency (NSTDA), Thailand, for financial support (Grant No. MT-B-55-CER-07-292-I) and the SUT-NANOTEC-SLRI joint

research facility for Synchrotron utilization for XAS beam time allocation.

References

1. S. Hassis, M. Santamouris, M. Papanikolaou, A. Linardi, N. Klitsikas, C. Georgakis, D.N. Assimakopoulos, *Energ. Buildings* 32 (2000) 131-141.
2. E. Stathopoulou, G. Mihalakakou, M. Santamouris, H.S. Bagiorgas, *J. Earth Syst. Sci.* 117 (2008) 227-236.
3. M. Santamouris, M. Papanikolaou, I. Livada, I. Koronakis, C. Georgakis, A. Argiriou, D.N. Assimakopoulos, *Sol. Energy* 70 (2001) 201-216.
4. M. Santamouris, M. Papanikolaou, G. Mihalakakou, *Climatic Change* 80 (2007) 265-276.
5. H. Akbari, H.D. Matthews, *Energ. Buildings* 55 (2012) 2-6.
6. M. Santamouris, A. Synnefa, T. Karlessi, *Sol. Energy* 85 (2011) 3085-3102.
7. T. Thongkanluang, T. Kittiauchawal, P. Limsuwan, *Ceram. Int.* 37 (2011) 543-548.
8. C. Ferrari, A. Muscio, C. Siligardi, T. Manfredini, *Ceram. Int.* 41 (2015) 11106-11116.
9. J. Zou, P. Zhang, C. Liu, Y. Peng, *Dyes Pigments* 109 (2014) 113-119.
10. V.S. Vishnu, G. George, M.L.P. Reddy, *Dyes Pigments* 85 (2010) 117-123.
11. V.S. Vishnu, M.L.P. Reddy, *Sol. Energ. Mat. Sol. C.* 95 (2011) 2685-2692.
12. G. George, V.S. Vishnu, M.L.P. Reddy, *Dyes Pigments* 88 (2011) 109-115.
13. K.J. Sreeram, C.P. Aby, B.U. Nair, T. Ramasami, *Sol. Energ. Mat. Sol. C.* 92 (2008) 1462-1467.
14. M. Newville, *J. Synchrotron Rad.* 8 (2001) 96-100.
15. B. Ravel, M. Newville, *J. Synchrotron Rad.* 12 (2005) 537-541.
16. R.D. Shannon, *Acta Crystallogr. Sect. A: Found. Crystallogr.* 32 (1976) 751-767.
17. J-C.G. Bünzli, C. Piguet, *Chem. Soc. Rev.* 34 (2005) 1048-1077.
18. K.J. Sreeram, R. Srinivasan, J.M. Devi, B.U. Nair, T. Ramasami, *Dyes and Pigments* 75 (2007) 687-692.